Bone Orientation and Position Estimation Errors Using Cosserat Point Elements and Least Squares methods: Application to Gait

Dana Solav [1,*], Valentina Camomilla [2,3], Andrea Cereatti [3,4,5], Arnaud Barré [6,7], Kamiar Aminian [7], Alon Wolf [1]

[1] Department of Mechanical Engineering, Technion Israel Institute of Technology, Haifa, Israel

[2] Department of Movement, Human and Health Sciences, University of Rome "Foro Italico", Rome, Italy

[3] Interuniversity Centre of Bioengineering of the Human Neuromusculoskeletal system, Rome, Italy

[4] POLCOMING Department, Information Engineering Unit, University of Sassari, Sassari, Italy

[5] Dept. of Electronics and Telecommunications, Politecnico di Torino, Torino, Italy

[6] Laboratoire de recherche en Imagerie et Orthopédie, École de Technologie Supérieure, H3C 1K3 Montréal, Canada

[7] Laboratory of Movement Analysis and Measurement, Ecole Polytechnique Fédérale de Lausanne, Lausanne, Switzerland

*Corresponding author. Tel: +972778875945, Fax: +972778875711, *E-mail:* danas@technion.ac.il

Submitted to the Journal of Biomechanics, September 2016. Accepted January 2017.

http://dx.doi.org/10.1016/j.jbiomech.2017.01.026

Abstract

The aim of this study was to analyze the accuracy of bone pose estimation based on sub-clusters of three skin-markers characterized by triangular Cosserat point elements (TCPEs) and to evaluate the capability of four instantaneous physical parameters, which can be measured non-invasively *in-vivo*, to identify the most accurate TCPEs. Moreover, TCPE pose estimations were compared with the estimations of two least squares minimization methods applied to the cluster of all markers, using rigid body (RBLS) and homogeneous deformation (HDLS) assumptions. Analysis was performed on previously collected *in-vivo* treadmill gait data composed of simultaneous measurements of the gold-standard bone pose by bi-plane fluoroscopy tracking the subjects' knee prosthesis and a stereophotogrammetric system tracking skin-markers affected by soft tissue artifact. Femur orientation and position errors estimated from skin-marker clusters were computed for 18 subjects using clusters of up to 35 markers. Results based on gold-standard data revealed that instantaneous subsets of TCPEs exist which estimate the femur pose with reasonable accuracy (median root mean square error during stance/swing: 1.4/2.8 deg for orientation, 1.5/4.2 mm for position). A non-invasive and instantaneous criteria to select accurate TCPEs for pose estimation (4.8/7.3 deg, 5.8/12.3 mm), was compared with RBLS (4.3/6.6 deg, 6.9/16.6 mm) and HDLS (4.6/7.6 deg, 6.7/12.5 mm). Accounting for homogeneous deformation, using HDLS or selected TCPEs, yielded more accurate position estimations than RBLS method, which, conversely, yielded more accurate orientation estimations. Further investigation is required to devise effective criteria for cluster selection that could represent a significant improvement in bone pose estimation accuracy.

Keywords: Bone Pose Estimation, Cosserat Point Theory, Human Movement Analysis, Soft Tissue Artifact, Stereophotogrammetry

1. Introduction

In the process of the estimation of a bone orientation and position (pose) from a marker cluster attached to the skin using optoelectronic stereophotogrammetry, the accuracy is greatly compromised by the relative motion between the skin markers and the underlying bone, which is defined in the literature as the soft tissue artifact (STA) (Leardini et al., 2005). STA is caused by a combination of skin stretching and sliding, muscle contractions, gravity and inertial effects (Leardini et al., 2005; Peters et al., 2010). Commonly used bone pose estimators (BPEs) define an appropriate marker cluster model and match the model with the measured marker trajectories at each time step by solving a least squares (LS) minimization problem constraining the cluster transformation to a translation and a rotation, with or without uniform scaling (Cappello et al., 1996; Challis, 1995; Söderkvist and Wedin, 1993; Spoor and Veldpaus, 1980). This technique has been implemented in numerous studies according to the framework of Procrustes analysis, and will be referred to in this paper as rigid body least squares (RBLS). Alternatively, the transformation can be approximated by a translation and a general non-singular tensor, which permits homogeneous deformation (including stretching and shearing). This approach was implemented in several studies under the framework of affine mapping (Ball and Pierrynowski, 1998; Dumas and Chèze, 2009; Solav et al., 2014), and will be referred to in this paper as homogeneous deformation least squares (HDLS). RBLS and HDLS generally obtain different results (Dumas and Chèze, 2009; Rubin and Solav, 2016; Solav et al., 2014).

The STA effects on a cluster can be decomposed into a rigid and a non-rigid component (Grimpampi et al., 2014). Various studies have shown that the rigid component is greater than the non-rigid component (Andersen et al., 2012; Barré et al., 2013; Benoit et al., 2015). Moreover, the rigid component has been demonstrated to be the only one impacting pose estimation accuracy when using RBLS (Bonci et al., 2015; Dumas et al., 2015; Grimpampi et al., 2014). This explains why commonly used BPEs based on RBLS, which compensate only for the non-rigid component (Cappozzo et al., 1997; Grimpampi et al., 2014; Heller et al., 2011; Söderkvist and Wedin, 1993; Veldpaus et al., 1988), are insufficient to fully compensate for the STA effects (Cereatti et al., 2006; Stagni and Fantozzi, 2009).

A recent work by some of the authors (Solav et al., 2016), presented a method based on the continuum mechanics theory of Cosserat, which evaluated the different poses estimated by all possible combinations of three-marker clusters characterized by triangular Cosserat point elements (TCPEs). At each time step, the strain in each TCPE, and the difference in the orientation and position estimations between pairs of TCPEs, were used to define three scalar TCPE parameters (E, ϕ, and T, respectively). These parameters are measured directly from the skin-marker trajectories and do not require gold-standard data. Although the TCPE parameters vanish when the entire cluster moves as a rigid body, and are therefore quantifying the non-rigidity of the entire cluster, the parameters ϕ and T contain information regarding the relative *rigid* transformation between sub-clusters. Therefore, they should not be strictly included in the same category as other STA non-rigid component definitions. It was hypothesized that TCPEs having small values of the parameters $\{E,\phi,T\}$ are more likely to accurately estimate the underlying bone pose. The correlations between each parameter and the pose estimation errors were evaluated using *ex-vivo* data measured on the lower limb of three cadavers having 12 skin-markers on the thigh and bone pins as gold-standard (Cereatti et al., 2009). The parameter ϕ showed to be the most correlated with the orientation error and the parameter T with the position error. Therefore, it was concluded that $\{\phi,T\}$ have the potential to identify TCPEs which more accurately estimate the bone orientation and position, respectively. However, the method was evaluated on a small *ex-vivo* dataset, and further research using comprehensive *in-vivo* data was required to better understand whether this approach can be effectively used for developing an accurate BPE.

The goal of this study is twofold: first, to explore using *in-vivo* gait data different criteria for non-invasive cluster selection based on the TCPE approach; and second, to compare the TCPE estimates with two different LS methods. The selection criteria are based upon four independent instantaneous parameters. Three are the above-mentioned parameters $\{E, \phi, T\}$. Since previous studies (Bonci et al., 2014; Camomilla et al., 2015, 2013) suggested that STA amplitudes linearly increase with proximal and distal joint kinematics, we hypothesized that the distance between the TCPE location and the most active joint may be used as a criterion for the selection of TCPEs least affected by STA. Therefore, a fourth parameter, named *active joint distance* parameter (D) was added to the analysis.

The evaluation was performed using gait data collected on 19 subjects, with simultaneous measurements of a stereophotogrammetric system tracking skin-markers and a bi-plane fluoroscopic system tracking the subjects' knee prosthesis as gold-standard reference (Barré et al., 2015, 2013). Since during gait the largest STA occurs on the thigh (Akbarshahi et al., 2010; Andersen et al., 2010; Barré et al., 2015; Benoit et al., 2006; Reinschmidt et al., 1997), the present methodology was evaluated by focusing on femur pose estimation.

2. Materials and Methods

2.1 Experimental setup

Data used in this study were collected by (Barré et al., 2015, 2013). A detailed description of the data collection and subjects was reported in these papers. In brief, a bi-plane fluoroscopic system (2 BV Pulsera 300, Philips, NL., sampled at 30 frames/s) and a seven-camera stereophotogrammetric system (MX3+, Vicon, U.K., sampled at 240 frames/s) were used simultaneously to measure the motion of the lower limbs during treadmill gait.

A total of 19 subjects (11 women and 8 men) with knee prosthesis (Symbios, CH) were evaluated. The mean ± standard deviation (SD) of age, mass, height and BMI were 70 ± 6 y.o., 80 ± 14 kg, 1.68 ± 0.09 m, and 28.4 ± 4.1 kg/m^2, respectively. A minimum of 35 spherical markers (Ø = 4 mm) were attached to the thigh skin, as illustrated in Fig. 1. A static trial in upright standing position and a 15s gait trial at comfortable speed (6.5 ± 1.1 m/s), corresponding to 6 to 10 gait cycles (GC), were recorded. The gold-standard femoral pose (orientation matrix $\boldsymbol{R}_{GS}$ and position vector $\boldsymbol{t}_{GS}^{(B)}$ of the anatomical coordinate systems (ACS)) was reconstructed from the fluoroscopic system, following the methods described in (Barré et al., 2013). The gold-standard ACS were defined using the femoral and tibial components of the prosthesis, as shown in Fig. 2.

Markers not visible due to occlusions in more than 25% of an entire trial were removed, and the remaining gaps were filled using generalized Procrustes analysis (Dryden and Mardia, 1998). Marker trajectories were downsampled to 30 frames/s to match the sample rate of the fluoroscopic system.

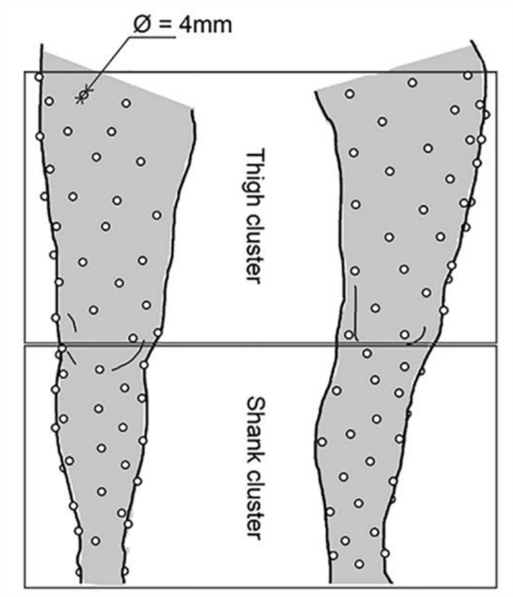

Fig. 1. Frontal (left) and sagittal (right) representation of the marker distribution for one specific subject.

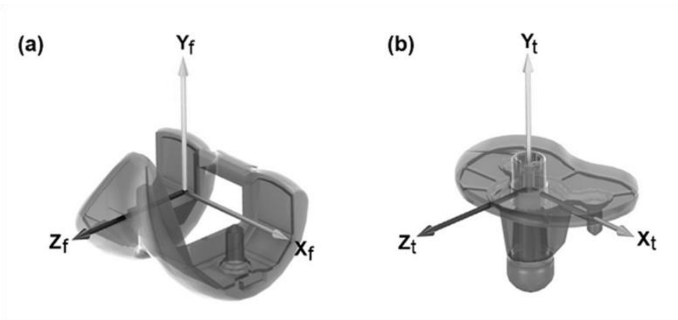

Fig. 2. Illustration of the femoral (a) and tibial (b) components of the prosthesis and the corresponding femoral and tibial anatomical coordinate systems (X_f, Y_f, Z_f and X_t, Y_t, Z_t , respectively).

2.2 TCPE pose estimation and parameters

The methods used in this study are based on previous works (Solav et al., 2016, 2014). The cluster of *M* skin-markers on the thigh was characterized by a group of *N* TCPEs based on all combinations of three markers, excluding those having a 2D isotropy index smaller than 0.5, which has been shown to cause large orientation errors (Cappozzo et al., 1997). For each TCPE, the marker cluster configuration during the static trial was used as the reference configuration. The position of the femur reference point *B* (Solav et al., 2016), was assumed to coincide with the origin of the femoral ACS in the reference configuration.

At each time step during the gait trials, and for each TCPE, the orientation and position estimations of the femoral ACS estimates were obtained, for each TCPE, by the non-rigid transformations from the reference configuration to each present configuration of the markers composing the TCPE. For each Jth TCPE, the transformation was estimated by a deformation gradient tensor $\boldsymbol{F}_J$ of the TCPE, and a translation vector $\boldsymbol{t}_J^{(B)}$ of point *B*. Moreover, the unique proper orthogonal rotation tensor $\boldsymbol{R}_J$ and the Lagrangian strain tensor $\boldsymbol{E}_J$ were obtained from $\boldsymbol{F}_J$, as described in (Solav et al., 2016).

The values of $\boldsymbol{E}_J$, $\boldsymbol{R}_J$, and $\boldsymbol{t}_J^{(B)}$ of each Jth TCPE were used to define, at each time step, three scalar parameters: E_J quantifying the magnitude of the strain, ϕ_J quantifying the average relative rotation angle between the Jth TCPE and all other TCPEs, and T_J quantifying the average relative translation between the Jth TCPE and all other TCPEs (Solav et al., 2016):

$$\begin{aligned} E_J &= \sqrt{\boldsymbol{E}_J \cdot \boldsymbol{E}_J} \\ \phi_J &= \frac{1}{N-1}\sum_{K=1}^{N} \cos^{-1}\left[\frac{1}{2}\left(\boldsymbol{R}_J \cdot \boldsymbol{R}_K - 1\right)\right] \\ T_J &= \frac{1}{N-1}\sum_{K=1}^{N} \left|\boldsymbol{t}_J^{(B)} - \boldsymbol{t}_K^{(B)}\right| , \end{aligned} \tag{1}$$

where $\boldsymbol{A}\cdot\boldsymbol{B} = tr(\boldsymbol{A}\boldsymbol{B}^T)$ is the inner product of two second order tensors $\{\boldsymbol{A},\boldsymbol{B}\}$.

In addition, a fourth parameter, named *active joint distance* parameter D_J, was defined for each Jth TCPE at each time step:

$$D_J = \theta_{Hip}\sum_{l=1}^{3}\left|\boldsymbol{x}_{Knee} - \boldsymbol{x}_l^{(J)}\right| + \theta_{Knee}\sum_{l=1}^{3}\left|\boldsymbol{x}_{Hip} - \boldsymbol{x}_l^{(J)}\right|, \tag{2}$$

where $\{\theta_{Hip}, \theta_{Knee}\}$ represent the estimated angular displacements at the hip and knee joints, computed in terms of rotation about the Euler axis at each time step with respect to the reference configuration, $\{\boldsymbol{x}_{Hip}, \boldsymbol{x}_{Knee}\}$ represent the estimated positions of the hip and knee joint centers, and $\boldsymbol{x}_l^{(J)}$ is the position of the l^{th} marker (l=1,2,3) of the Jth TCPE. This parameter is defined such that the value of D_J increases if the Jth TCPE is located closer to a joint that undergoes a large angular displacement with respect to the reference configuration.

The four TCPE parameters $\{E, \phi, T, D\}$ were computed for each TCPE at each time step using only the skin marker trajectories, and were used for selecting, at each time step, groups of TCPEs having the smallest values of these parameters out of the group of all TCPEs.

The gold-standard pose (orientation $\boldsymbol{R}_{GS}$ and position $\boldsymbol{t}_{GS}^{(B)}$) was used to compute the orientation error $\Delta\theta_J$ and the position error Δt_J for each Jth TCPE at each time step, by

$$\Delta\theta_J = \cos^{-1}\left[\frac{1}{2}\left(\boldsymbol{R}_J \cdot \boldsymbol{R}_{GS} - 1\right)\right]\ ;\ \Delta t_J = \left|\boldsymbol{t}_J^{(B)} - \boldsymbol{t}_{GS}^{(B)}\right|. \tag{3}$$

2.3 Pose estimation by least squares (LS) methods

In general, the transformation of each skin-marker i, from its reference position $\boldsymbol{X}_i$ to its present position $\boldsymbol{x}_i$, measured relative to a fixed point (measured in the global coordinate system), can be described by

$$\boldsymbol{x}_i = \boldsymbol{X}^{(B)} + \boldsymbol{t}^{(B)} + \boldsymbol{Q}\left(\boldsymbol{X}_i - \boldsymbol{X}^{(B)}\right), \tag{4}$$

where $\boldsymbol{X}^{(B)}$ is the position vector of reference point B (the femur's ACS origin measured in the reference static configuration), $\boldsymbol{Q}$ is a second order tensor which represents the transformation of line elements between the two configurations, and $\boldsymbol{t}^{(B)}$ is the translation vector of point B. In the presence of STA, Eq. (4) cannot be satisfied exactly for each i^{th} marker $(i = 1...M\ ;\ M \geq 3)$ of the cluster. Commonly used BPEs obtain the values of the best-fit $\boldsymbol{Q}$ and $\boldsymbol{t}^{(B)}$ by solving the LS minimization problem

$$\min \sum_{i=1}^{M} \left\| \boldsymbol{X}^{(B)} + \boldsymbol{t}^{(B)} + \boldsymbol{Q}\left(\boldsymbol{X}_i - \boldsymbol{X}^{(B)}\right) - \boldsymbol{x}_i \right\|^2 . \tag{5}$$

As discussed in the introduction, the RBLS approach consists in assuming that $\boldsymbol{Q} = \boldsymbol{R}_{(RB)}$ be a proper orthogonal rotation tensor that satisfies the constraint

$$\boldsymbol{R}_{(RB)}^T \boldsymbol{R}_{(RB)} = \boldsymbol{I} ,\ \det\left(\boldsymbol{R}_{(RB)}\right) = 1 . \tag{6}$$

Consequently, the estimated orientation of the bone is $\boldsymbol{R}_{(RB)}$, and its estimated position is obtained by

$$\boldsymbol{t}_{(RB)}^{(B)} = \boldsymbol{x}_{(RB)}^{(B)} - \boldsymbol{X}^{(B)} = \bar{\boldsymbol{x}} - \boldsymbol{R}_{(RB)}\left(\bar{\boldsymbol{X}} - \boldsymbol{X}^{(B)}\right) - \boldsymbol{X}^{(B)} , \tag{7}$$

where $\left\{\bar{\boldsymbol{X}}, \bar{\boldsymbol{x}}\right\}$ are the centroids of the reference and present marker-cluster configurations $\left\{\boldsymbol{X}_i, \boldsymbol{x}_i\right\}$, respectively.

Conversely, using HDLS, $\boldsymbol{Q} = \boldsymbol{Q}_{(HD)}$ can be a general second order tensor with a positive determinant, which contains homogeneous deformation. In this case, Eq. (6) is no longer valid and the estimated bone orientation is obtained by decomposing $\boldsymbol{Q}_{(HD)}$ to obtain the unique orthogonal rotation tensor $\boldsymbol{R}_{(HD)}$ using the polar decomposition (Veldpaus et al., 1988), singular value decomposition (Söderkvist and Wedin, 1993), or eigenvalue decomposition (Spoor and Veldpaus, 1980). All three options analytically provide the same result (Solav et al., 2016), although small numerical differences may occur if the markers are badly configured. Consequently, the estimated bone position is obtained by

$$\boldsymbol{t}_{(HD)}^{(B)} = \boldsymbol{x}_{(HD)}^{(B)} - \boldsymbol{X}^{(B)} = \bar{\boldsymbol{x}} - \boldsymbol{Q}_{(HD)}\left(\bar{\boldsymbol{X}} - \boldsymbol{X}^{(B)}\right) - \boldsymbol{X}^{(B)} . \tag{8}$$

Note that using HDLS, vectors can stretch and not only rotate by the tensor $\boldsymbol{Q}_{(HD)}$. Therefore, the position estimation $\boldsymbol{t}_{(HD)}^{(B)}$ may be different than $\boldsymbol{t}_{(RB)}^{(B)}$ even if $\boldsymbol{R}_{(HD)} = \boldsymbol{R}_{(RB)}$.

For comparison, the values of the orientation errors $\left\{\Delta\theta_{(RB)}, \Delta\theta_{(HD)}\right\}$ and position errors $\left\{\Delta t_{(RB)}, \Delta t_{(HD)}\right\}$ obtained by applying RBLS and HDLS to the cluster of all markers were computed as their angular and linear displacements relative to the gold-standard pose, similarly to Eq. (3).

2.4 **Data analysis**

The instantaneous orientation and position errors were obtained for all the TCPEs and for the RBLS and HDLS methods. The root mean square (RMS) errors were computed for each subject, separately for the stance phase (0-60% of each GC) and swing phase (60-100% of each GC). To examine the potential of the TCPE parameters to identify the TCPEs estimating the most accurate orientation and position, the time-variant values of the Spearman's rank correlation coefficients $\left(r_s\right)$ between the pose errors and each of the instantaneous TCPE parameters were calculated.

Descriptive statistics of the values of the pose errors and of the correlation coefficients were obtained, after a normal distribution test, using the five-number summary technique (minimum, lower quartile, median, upper quartile, and maximum), and data were represented using box-plots. Lower and upper quartiles were used to calculate the inter-quartile range (IQR).

Furthermore, instantaneous selection of groups of TCPEs having the smallest values of TCPE parameters was performed. The selection is based on skin marker data only, and therefore can be used non-invasively *in-vivo*. The orientation and position errors obtained by the selected TCPEs were compared with those obtained using the RBLS and HDLS methods.

3. **Results**

Subject number 8 from the original data set was excluded due to a reduced number of visible markers on the thigh. Following the marker exclusion procedure, described in section 2.1, the number of used thigh markers became 26.1 ± 5.4. Furthermore, following the TCPE exclusion criterion, described in section 2.2, the number of TCPEs was reduced to 394 ± 198.

Statistical values of the orientation and position errors $\{\Delta\theta, \Delta t\}$ for all TCPEs are shown in Fig. 3 for one cycle of four subjects, which were selected such that they represent the wide variety between the subjects. The temporal behavior of the errors for all subjects is provided in Fig. 1s of the supplementary material. The wide ranges of the errors obtained by different TCPEs indicate that the STA is highly inhomogeneous. The TCPEs which estimated the most accurate instantaneous pose, determined using gold-standard data, were different for orientation and position and varied between time steps. Across all subjects, the number of different TCPEs which estimated the most accurate instantaneous pose ranged between 35 and 150 for orientation and between 43 and 136 for position. The number of markers which composed these TCPEs ranged between 18 and 34, which represented 94 ± 8 % of the total number of markers.

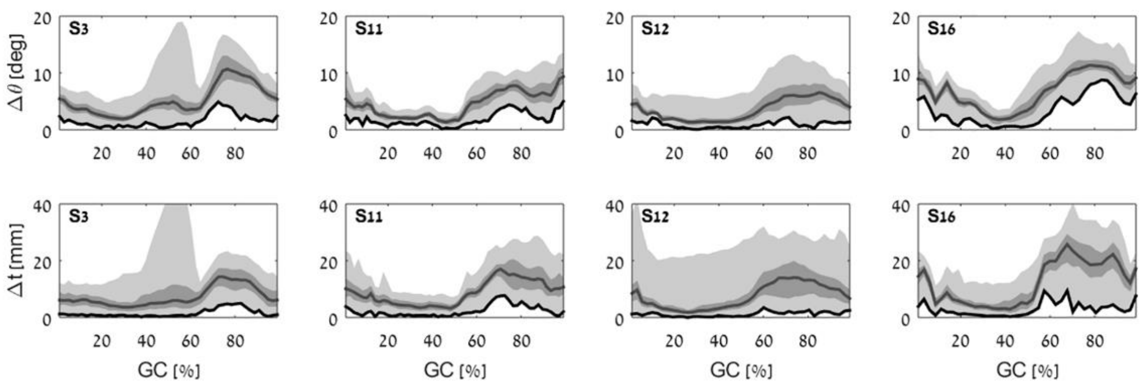

Fig. 3. Statistics of the orientation errors ($\Delta\theta_J$) and position errors (Δt_J) obtained by all TCPEs for one gait cycle (GC) of four different subjects (subject numbers 3, 11, 12, and 16 in the original dataset): minimum (black line), median (dark grey line), 25th-75th percentiles (grey band), and range (light grey band).

Statistical values of the correlation coefficients r_s between each TCPE parameter and the pose errors are presented in Fig. 4. The strain parameter *E* exhibited weak correlations with the errors, with median (IQR) values of 0.27 (0.11) with the orientation error and 0.34 (0.11) with the position error. The rotational parameter ϕ exhibited moderate correlations with the orientation error (0.49 (0.14)) and weak correlations with the position error (0.39 (0.14)). The translational parameter *T* exhibited weak to moderate correlations with the orientation error (0.40 (0.10)) and strong correlations with the position error (0.71 (0.10)), and the location parameter *D* exhibited weak correlations with the orientation and position errors (0.31 (0.12) and 0.34 (0.17), respectively).

The correlation results revealed that ϕ was the most correlated with $\Delta\theta$, though not strongly correlated, and that T was the most correlated with Δt. Therefore, we expected that in order to reduce the errors $\{\Delta\theta, \Delta t\}$, the TCPEs having the smallest values of ϕ and T, respectively, must be selected.

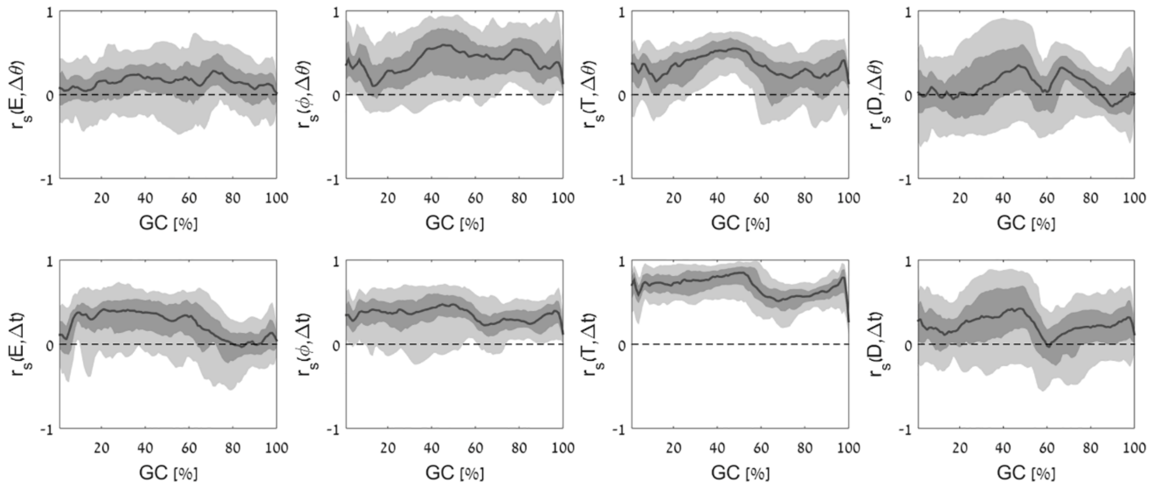

Fig. 4. Median (black line), 25th-75th percentiles (dark grey band), and 5th-95th percentiles (light grey band) values of Spearman correlation coefficients between TCPE parameters $\{E_J, \phi_J, T_J, D_J\}$ and the associated pose errors $\{\Delta\theta, \Delta t\}$. Statistics performed over 143 GC (18 subjects, 6 to 10 cycles each).

The orientation errors obtained by the non-invasive instantaneous selection of five TCPEs having the smallest values of ϕ and the position errors obtained by selecting five TCPEs having the smallest values of T, are presented in Fig. 5, for the same four cycles as in Fig. 3. The estimation errors obtained by applying the RBLS and HDLS methods to the cluster of all markers are plotted for comparison. Moreover, statistics of the RMS errors obtained over all subjects by the non-invasive TCPE selections, by the most accurate TCPEs obtained using gold-standard data, and by the RBLS and HDLS methods, are given in Fig. 6, separately for the stance and swing phases. Pose estimation errors during swing were substantially larger than during stance for all subjects, regardless of the estimation method. On average, during swing orientation estimation errors were 58% larger and position estimation errors were 106% larger compared with those obtained during stance. The temporal behavior and RMS values of the estimation errors for all subjects are reported in the online supplementary material, in Fig. 2s and Table 1s, respectively.

Instantaneous selection of five TCPEs with the smallest values of T obtained smaller position RMS errors than those obtained by RBLS, over the entire duration of the trial, in all subjects except one. The mean ± SD of the RMS error reduction over all subjects was 18.5 ± 8.2%. Error reduction during the swing phase was more substantial, and was obtained in all subjects (22.0 ± 13.4%). Note that we chose to present here the error reduction relative to RBLS, on account of it being the most commonly used BPE. HDLS achieved comparable position estimation errors to those obtained by non-invasive TCPE selection during swing (20.3 ± 16.7% reduction), but not during stance (6.0 ± 23.4% larger than RBLS). Conversely, RBLS was more accurate than HDLS in estimating the orientation (HDLS errors 14.3 ± 15.7% larger than RBLS). This difference was also more substantial (20.4 ±

19.2%) and consistent (in all subjects) during swing. Selection of five TCPEs with smallest values of ϕ did not provide orientation error reduction compared with the LS methods (9.3 ± 8.1% larger than RBLS and 2.8 ± 10.8% smaller than HDLS). Subject specific differences between methods can be derived from Table 1s.

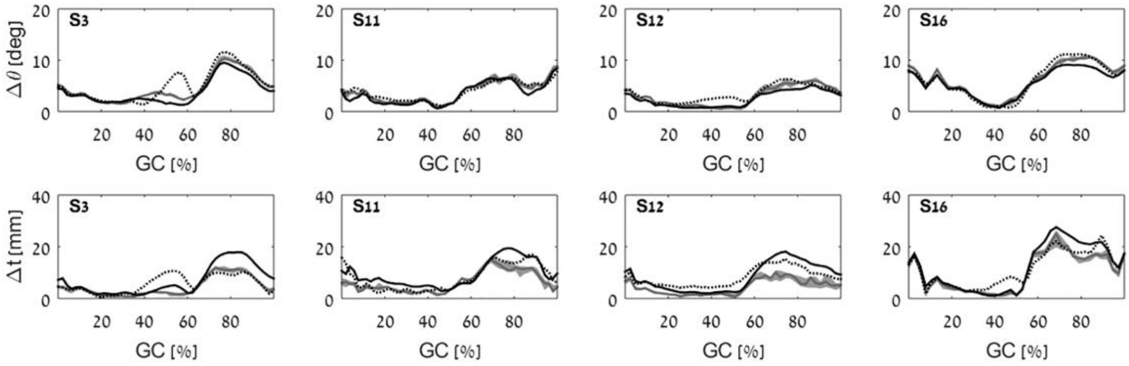

Fig. 5. Statistics of the orientation errors $(\Delta\theta_J)$ for the 5 TCPEs having the smallest ϕ_J and position errors (Δt_J) for the 5 TCPEs having the smallest T_J (median: dark grey, range: grey), and the errors obtained by applying the RBLS and HDLS methods to the cluster of all markers (solid and dotted black lines, respectively), for one GC of four different subjects (same as in Fig. 3).

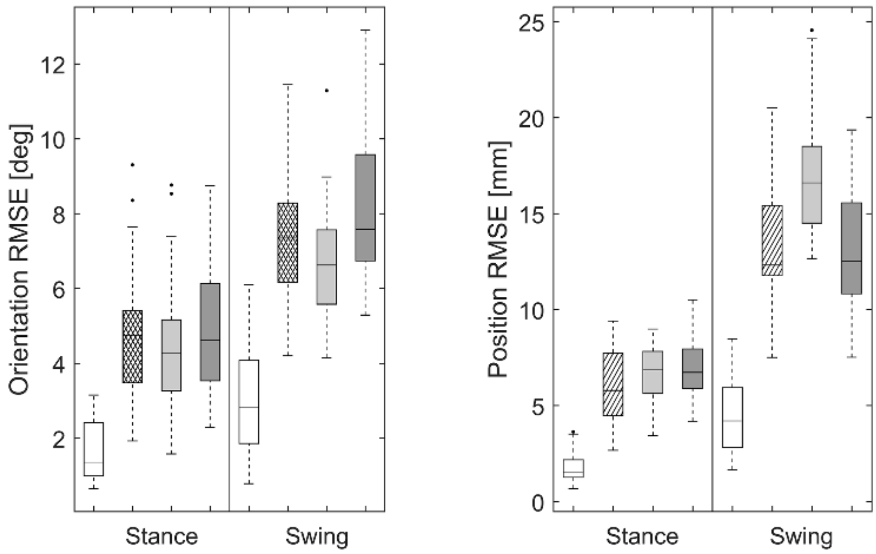

Fig. 6. Boxplots (median, 25th-75th percentiles, minimum and maximum, and outliers) of the RMS values of the orientation and position errors obtained over all subjects, for the stance and swing phases, and for each method: The most accurate TCPE (white), 5 TCPEs selected with the smallest ϕ parameter (white cross fill), 5 TCPEs selected with the smallest *T* parameter (white stripe fill), RBLS method (light grey), and HDLS method (dark grey).

4. **Discussion**

This study evaluated the proposed TCPE method using comprehensive *in-vivo* treadmill gait data, and compared it with two LS minimization approaches. Femur orientation and position errors obtained by different TCPEs were analyzed in terms of four instantaneous parameters, which can be measured non-invasively and *in-*

vivo. Pose errors estimated by all methods were substantially larger during swing than during stance. This finding is in accordance with the individual marker displacements reported by (Barré et al., 2015) using the same data, as well as with the findings of (Akbarshahi et al., 2010) concerning knee joint rotation errors obtained from four young healthy subjects. A small portion of the large errors during swing can also be explained by possible blur of the X-ray images due to the pulse duration time which could reduce the quality of the prostheses model fitting (Barré et al., 2013).

The orientation and position errors obtained by different TCPEs exhibited high variability, which indicated that the STA is highly inhomogeneous. It was shown that, if the most accurate TCPEs could be identified at each time step, the orientation and position errors would be reasonably small, especially during stance. This result confirms that there is no synchronous rigid motion of the *entire* cluster relative to the underlying bone (Camomilla et al., 2009; Solav et al., 2016), and that instantaneous optimal selection of sub-clusters has the potential to greatly reduce pose estimation errors. The TCPEs which obtained the smallest pose estimation errors varied greatly across time and between orientation and position, and were composed of almost all markers. Therefore, it was not feasible to identify specific optimal subsets of TCPEs, or optimal markers, for the entire duration of the trials. These findings justify the use of a cluster containing a large number of markers and the instantaneous selection of sub-clusters, for estimating more accurate orientation and position. The large variability in the number of TCPEs across subjects was caused by two major reasons: first, the different number of visible markers led to a large variability in the initial number of TCPEs due to the nature of the combination formula; and second, the number of TCPEs excluded by the isotropy index condition was highly affected by differences in the relative positions between the markers.

To examine criteria for optimal TCPE selection, the instantaneous correlation coefficients between the TCPE parameters and the pose errors were computed. Strong correlations were found only between the translational parameter T and the position estimation error for all subjects and all gait cycles. Conversely, moderate correlations were found between the rotational parameter ϕ and the orientation estimation error. These results, as well as the weak correlation found for the strain parameter E are in partial agreement with a previous *ex-vivo* study (Solav et al., 2016). Furthermore, the *active joint distance* parameter D was not effective for accurate TCPE selection, despite the known functional relationship between proximal and distal joint kinematics and the STA effects (Bonci et al., 2014), possibly due to the combined effects of the hip and knee joint movements. This finding suggests that one global parameter is insufficient as a selection criterion for TCPEs.

The instantaneous orientation and position errors obtained by five TCPEs selected non-invasively according to the smallest values of T and ϕ, respectively, were compared with those obtained by two LS methods. Orientation errors estimated by the selected TCPEs were smaller than those obtained by HDLS and larger than those obtained by RBLS. However, these differences were not substantial. HDLS obtained larger orientation estimation errors than RBLS in most of the subjects. Position errors estimated by the selected TCPEs were considerably smaller than those obtained by RBLS, especially during swing. Moreover, they were comparable with HDLS during swing and smaller than HDLS during stance. These findings indicate that accounting for homogeneous deformation and thus allowing lines to stretch and not only rotate when calculating the bone's position (see Eq. 8), results in more accurate position estimation. Moreover, these results justify using either HDLS or TCPE for reducing the position estimation errors. However, since RBLS obtained smaller orientation errors, the use of HDLS and TCPE methods should be applied for the estimation of position and not of orientation.

It is therefore suggested that different estimation methods be used separately for position and orientation estimations.

The results revealed that, during gait, only the position estimation accuracy can be improved by non-invasively selecting TCPEs having the smallest values of *T*. The findings suggest that TCPEs having low values of ϕ rotate in quasi-unison with the movement of the cluster of all markers estimated by the LS methods and are therefore incapable of improving the orientation estimation accuracy. Conversely, TCPEs having low values of *T* translate relative to the cluster of all markers and follow more closely the position of the underlying bone.

This study also entails some limitations. First, the results are limited to a specific population and motor task (elderly people who underwent total knee arthroplasty during treadmill gait at a relatively slow speed). Further investigations using different experimental conditions should determine if these results can be generalized. Secondly, the estimation accuracy was obtained by applying the LS methods to a highly redundant number of markers. However, in clinical practice this is rarely the case. Since it has been suggested that large number of markers may improve the accuracy of BPEs (Cereatti et al., 2006) and decrease differences associated to cluster design (Barré et al., 2015), caution should be taken in generalizing the specific results to clusters containing fewer markers.

In conclusion, the results revealed the existence of TCPEs which estimated the underlying bone pose fairly accurately. However, the proposed criteria for the instantaneous non-invasive selection of these TCPEs, was effective only for reducing the position errors, while RBLS obtained smaller orientation estimation errors. The results justify using sub-groups of TCPEs having small values of the TCPE parameter *T* for estimating position and RBLS estimating orientation. Moreover, the findings justify further investigations to devise improved criteria for cluster selection that would represent significant improvement in bone pose estimation accuracy.

Appendix A. Supplementary information

Table 1s. RMS orientation and position errors estimated during the stance and swing phases for each subject and statistics for all subjects. Subject number 8 from the original data set was excluded due to a reduced number of visible thigh markers. Statistical values are presented as minimum (Min), lower quartile (LQ), median (Med), upper quartile (UQ), maximum (Max), and inter-quartile range (IQR). Four different estimations are presented: the most accurate TCPE (TCPE min), a subset of 5 TCPEs selected by the smallest TCPE parameters (ϕ for orientation and T for position), HDLS method, and RBLS method.

			Subjects																		Statistics					
Error	**Phase**	**Method**	**1**	**2**	**3**	**4**	**5**	**6**	**7**	**9**	**10**	**11**	**12**	**13**	**14**	**15**	**16**	**17**	**18**	**19**	**Min**	**LQ**	**Med**	**UQ**	**Max**	**IQR**
Orientation [deg]	Stance	**TCPE min**	1.4	0.7	1.0	3.1	1.2	2.5	1.3	2.4	0.7	1.3	1.0	1.7	1.1	2.4	2.4	1.0	3.2	2.0	0.7	1.0	1.4	2.4	3.2	1.4
		TCPE select Φ	5.4	3.6	2.8	8.4	3.5	9.3	4.7	5.3	2.7	2.9	1.9	3.5	4.7	5.6	5.1	5.2	7.6	4.8	1.9	3.5	4.8	5.4	9.3	1.9
		HDLS	5.7	4.3	3.3	7.5	3.9	8.3	4.6	6.1	2.8	3.3	2.3	3.5	4.2	5.2	4.6	4.8	8.7	8.3	2.3	3.5	4.6	6.1	8.7	2.6
		RBLS	5.6	3.9	2.6	8.5	3.3	8.8	4.2	4.9	2.5	2.6	1.6	3.6	4.3	5.2	4.8	5.0	7.4	4.0	1.6	3.3	4.3	5.2	8.8	1.9
	Swing	**TCPE min**	0.8	1.1	2.7	5.3	1.9	2.7	1.5	4.0	2.4	3.4	1.5	3.0	4.1	2.0	6.1	3.6	4.1	5.0	0.8	1.9	2.8	4.1	6.1	2.2
		TCPE select Φ	5.4	4.2	7.7	11.5	5.5	9.4	8.0	7.2	7.5	6.2	5.1	6.2	6.6	6.5	9.1	9.5	8.1	8.3	4.2	6.2	7.3	8.3	11.5	2.1
		HDLS	6.7	5.8	8.4	11.9	5.8	9.9	8.9	7.6	7.6	5.9	5.3	7.1	7.0	7.1	9.6	9.6	10.4	12.9	5.3	6.7	7.6	9.6	12.9	2.8
		RBLS	4.9	4.2	6.9	11.3	4.5	9.0	6.6	6.4	6.8	5.9	4.2	5.9	6.6	5.6	8.2	8.3	7.6	7.0	4.2	5.6	6.6	7.6	11.3	2.0
Position [mm]	Stance	**TCPE min**	2.1	1.2	0.9	1.8	1.9	1.3	3.5	0.9	0.7	1.5	1.3	1.5	1.4	1.5	2.6	2.2	3.6	2.3	0.7	1.3	1.5	2.2	3.6	0.9
		TCPE select T	7.7	4.5	2.7	8.5	6.8	9.4	8.4	4.0	3.9	4.6	3.2	5.4	4.9	5.1	6.8	9.0	7.2	6.2	2.7	4.5	5.8	7.7	9.4	3.3
		HDLS	6.5	8.0	4.2	6.1	9.4	7.5	7.0	4.4	4.6	5.9	5.8	7.3	6.1	6.5	7.6	9.9	8.2	10.5	4.2	5.9	6.7	8.0	10.5	2.0
		RBLS	8.0	6.3	3.4	5.4	9.0	6.4	8.7	6.9	5.0	6.9	4.7	6.8	6.0	5.6	7.3	8.9	7.8	7.7	3.4	5.6	6.9	7.8	9.0	2.2
	Swing	**TCPE min**	2.5	4.6	2.8	3.6	2.3	1.7	3.6	4.2	6.7	4.6	2.2	8.4	5.1	4.2	5.9	8.5	4.2	8.5	1.7	2.8	4.2	5.9	8.5	3.1
		TCPE select T	10.7	12.3	8.4	11.8	12.0	12.2	11.8	12.4	13.1	10.4	7.5	18.3	15.4	14.1	17.3	20.5	13.2	18.8	7.5	11.8	12.3	15.4	20.5	3.6
		HDLS	9.7	10.8	7.5	14.2	10.5	12.9	11.5	10.5	13.8	12.7	12.1	19.4	15.6	12.4	18.7	17.0	11.3	17.2	7.5	10.8	12.5	15.6	19.4	4.7
		RBLS	14.4	12.7	13.2	17.5	14.5	14.7	16.6	18.5	16.6	14.6	14.2	21.6	17.7	15.8	21.6	24.1	17.1	24.6	12.7	14.5	16.6	18.5	24.6	4.0

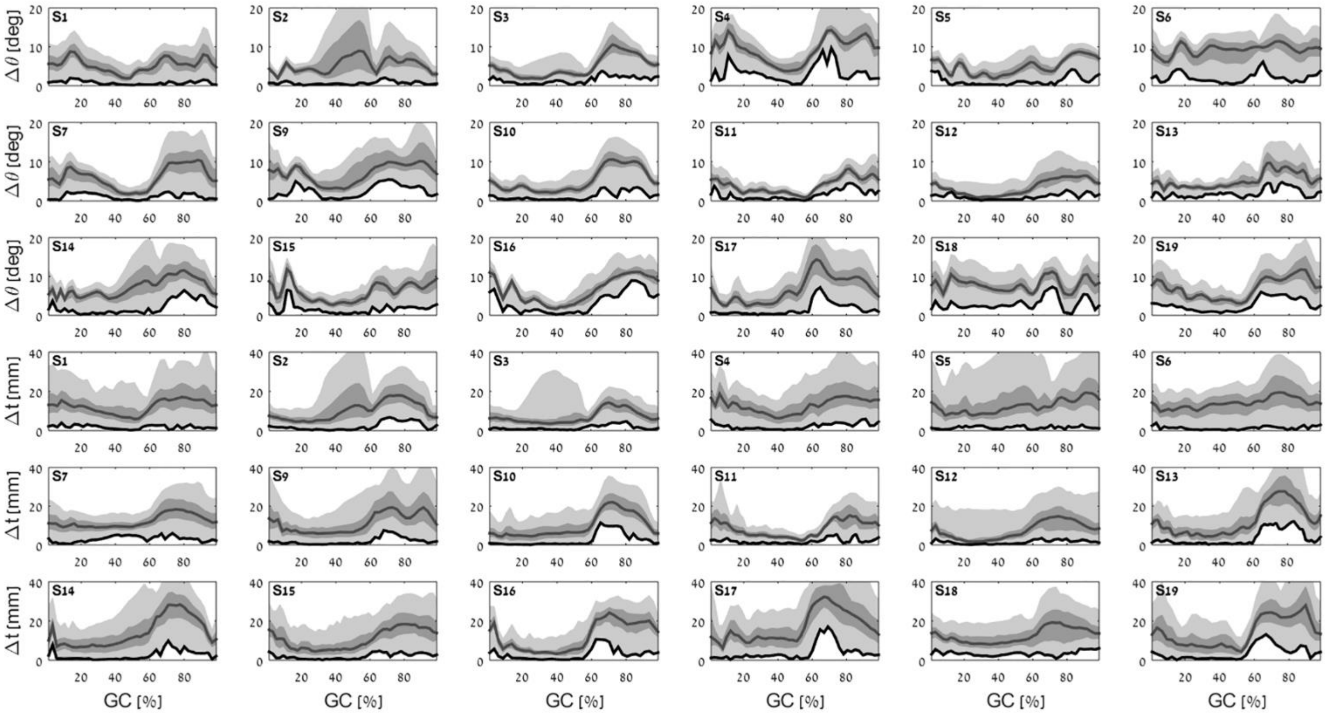

Fig. 1s. Statistics of the orientation errors ($\Delta\theta_J$) and position errors (Δt_J) obtained by all TCPEs: minimum (black line), median (dark grey line), 25th-75th percentiles (grey band), and range (light grey band). Results are shown for one cycle for each subject.

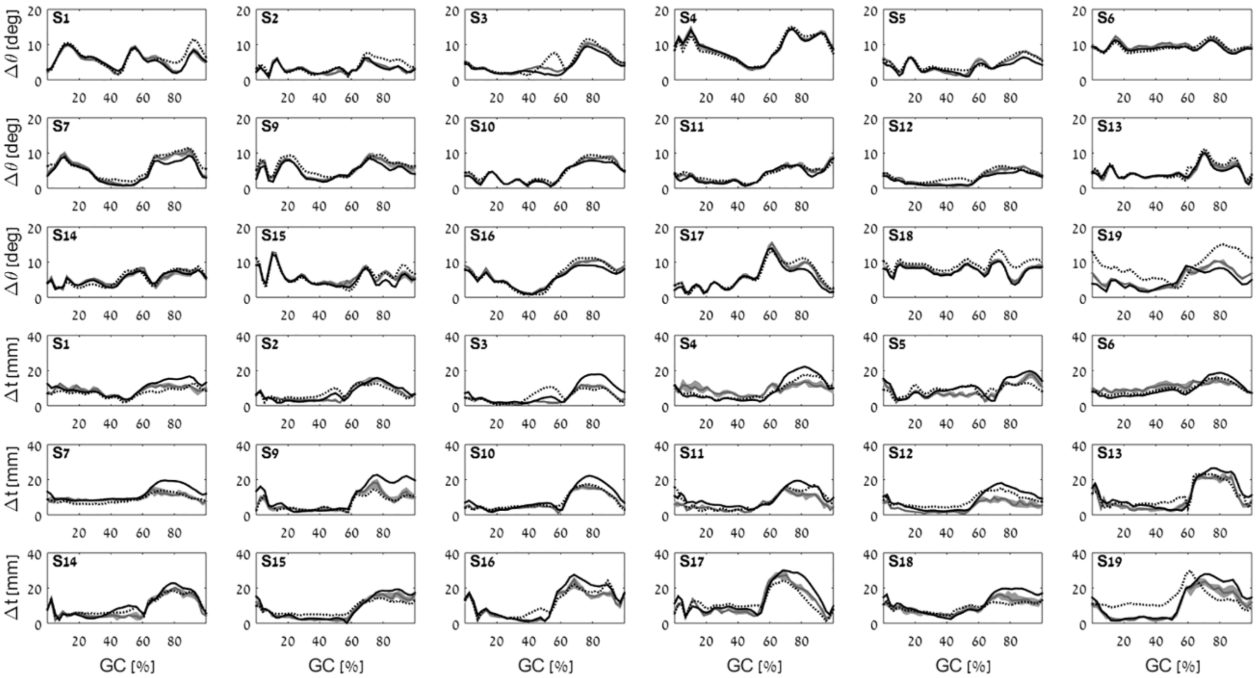

Fig. 2s. Statistics of the orientation errors ($\Delta\theta_J$) for the 5 TCPEs having the smallest ϕ_J and position errors (Δt_J) for the 5 TCPEs having the smallest T_J (median: dark grey, range: grey), and the errors obtained by applying the RBLS and HDLS methods on the cluster of all markers (solid and dotted black lines, respectively). Results are shown for one cycle for each subject.

References

Akbarshahi, M., Fernandez, J., Schache, A., Baker, R., Banks, S., MG, P., 2010. Non-invasive assessment of soft tissue artifact and its effect on knee joint kinematics during functional activity. J. Biomech. 43, 1292–1301.

Andersen, M.S., Benoit, D.L., Damsgaard, M., Ramsey, D.K., Rasmussen, J., 2010. Do kinematic models reduce the effects of soft tissue artefacts in skin marker-based motion analysis? An in vivo study of knee kinematics. J. Biomech. 43, 268–273. doi:10.1016/j.jbiomech.2009.08.034

Andersen, M.S., Damsgaard, M., Rasmussen, J., Ramsey, D.K., Benoit, D.L., 2012. A linear soft tissue artefact model for human movement analysis: Proof of concept using in vivo data. Gait Posture 35, 606–611. doi:10.1016/j.gaitpost.2011.11.032

Ball, K.A., Pierrynowski, M.R., 1998. Modeling of the pliant surfaces of the thigh and leg during gait, in: Proceedings of SPIE- BiOS'98 International Biomedical Optics Symposium. International Society for Optics and Photonics, pp. 435–446. doi:10.1117/12.308193

Barré, A., Jolles, B.M., Theumann, N., Aminian, K., 2015. Soft tissue artifact distribution on lower limbs during treadmill gait: Influence of skin markers' location on cluster design. J. Biomech. 48, 1965–71. doi:10.1016/j.jbiomech.2015.04.007

Barré, A., Thiran, J.P., Jolles, B.M., Theumann, N., Aminian, K., 2013. Soft tissue artifact assessment during treadmill walking in subjects with total knee arthroplasty. IEEE Trans. Biomed. Eng. 60, 3131–3140. doi:10.1109/TBME.2013.2268938

Benoit, D.L., Damsgaard, M., Andersen, M.S., 2015. Surface marker cluster translation, rotation, scaling and deformation: Their contribution to soft tissue artefact and impact on knee joint kinematics. J. Biomech. 48, 2124–2129. doi:10.1016/j.jbiomech.2015.02.050

Benoit, D.L., Ramsey, D.K., Lamontagne, M., Xu, L., Wretenberg, P., Renström, P., 2006. Effect of skin movement artifact on knee kinematics during gait and cutting motions measured in vivo. Gait Posture 24, 152–164. doi:10.1016/j.gaitpost.2005.04.012

Bonci, T., Camomilla, V., Dumas, R., Chéze, L., Cappozzo, A., 2015. Rigid and non-rigid geometrical transformations of a marker-cluster and their impact on bone-pose estimation. J. Biomech. 48, 4166–4172. doi:10.1016/j.jbiomech.2015.10.031

Bonci, T., Camomilla, V., Dumas, R., Chéze, L., Cappozzo, A., 2014. A soft tissue artefact model driven by proximal and distal joint kinematics. J. Biomech. 47, 2354–2361. doi:10.1016/j.jbiomech.2014.04.029

Camomilla, V., Bonci, T., Dumas, R., Chéze, L., Cappozzo, A., 2015. A model of the soft tissue artefact rigid component. J. Biomech. 48, 1752–1759. doi:10.1016/j.jbiomech.2015.05.007

Camomilla, V., Cereatti, A., Chèze, L., Cappozzo, A., 2013. A hip joint kinematics driven model for the generation of realistic thigh soft tissue artefacts. J. Biomech. 46, 625–630. doi:10.1016/j.jbiomech.2012.09.018

Camomilla, V., Donati, M., Stagni, R., Cappozzo, A., 2009. Non-invasive assessment of superficial soft tissue local displacements during movement: A feasibility study. J. Biomech. 42, 931–937. doi:10.1016/j.jbiomech.2009.01.008

Cappello, A., La Palombara, P.F., Leardini, A., 1996. Optimization and smoothing techniques in movement analysis. Int. J. Biomed. Comput. 41, 137–151. doi:10.1016/0020-7101(96)01167-1

Cappozzo, A., Cappello, A., Della Croce, U., Pensalfini, F., 1997. Surface-maker cluster design criteria for 3-D bone movement reconstruction. IEEE Trans. Biomed. Eng. 44, 1165–1174. doi:10.1109/10.649988

Cereatti, A., Della Croce, U., Cappozzo, A., 2006. Reconstruction of skeletal movement using skin markers: comparative assessment of bone pose estimators. J. Neuroeng. Rehabil. 3, 7. doi:10.1186/1743-0003-3-7

Cereatti, A., Donati, M., Camomilla, V., Margheritini, F., Cappozzo, A., 2009. Hip joint centre location: An ex vivo study. J. Biomech. 42, 818–823. doi:10.1016/j.jbiomech.2009.01.031

Challis, J.H., 1995. A procedure for determining rigid body transformation parameters. J. Biomech. 28, 733–737. doi:10.1016/0021-9290(94)00116-L

Dryden, L., Mardia, K. V, 1998. Statistical Shape Analysis, John Wiley & Son.

Dumas, R., Camomilla, V., Bonci, T., Chèze, L., Cappozzo, A., 2015. What portion of the soft tissue artefact requires compensation when estimating joint kinematics? J. Biomech. Eng. 137, 64502. doi:10.1115/1.4030363

Dumas, R., Chèze, L., 2009. Soft tissue artifact compensation by linear 3D interpolation and approximation methods. J. Biomech. 42, 2214–2217. doi:10.1016/j.jbiomech.2009.06.006

Grimpampi, E., Camomilla, V., Cereatti, A., De Leva, P., Cappozzo, A., 2014. Metrics for describing soft-tissue artefact and its effect on pose, size, and shape of marker clusters. IEEE Trans. Biomed. Eng. 61, 362–367. doi:10.1109/TBME.2013.2279636

Heller, M.O., Kratzenstein, S., Ehrig, R.M., Wassilew, G., Duda, G.N., Taylor, W.R., 2011. The weighted optimal common shape technique improves identification of the hip joint center of rotation in vivo. J. Orthop. Res. 29, 1470–1475. doi:10.1002/jor.21426

Leardini, A., Chiari, A., Della Croce, U., Cappozzo, A., 2005. Human movement analysis using stereophotogrammetry Part 3. Soft tissue artifact assessment and compensation. Gait Posture 21, 212–225. doi:10.1016/j.gaitpost.2004.05.002

Peters, A., Galna, B., Sangeux, M., Morris, M., Baker, R., 2010. Quantification of soft tissue artifact in lower limb human motion analysis: A systematic review. Gait Posture 31, 1–8. doi:10.1016/j.gaitpost.2009.09.004

Reinschmidt, C., Van Den Bogert, A.J., Lundberg, A., Nigg, B.M., Murphy, N., Stacoff, A., Stano, A., 1997. Tibiofemoral and tibiocalcaneal motion during walking: External vs. Skeletal markers. Gait Posture 6, 98–109. doi:10.1016/S0966-6362(97)01110-7

Rubin, M.B., Solav, D., 2016. Unphysical properties of the rotation tensor estimated by least squares optimization with specific application to biomechanics. Int. J. Eng. Sci. 103, 11–18. doi:10.1016/j.ijengsci.2016.02.001

Söderkvist, I., Wedin, P.Å., 1993. Determining the movements of the skeleton using well-configured markers. J. Biomech. 26, 1473–1477. doi:10.1016/0021-9290(93)90098-Y

Solav, D., Rubin, M.B., Cereatti, A., Camomilla, V., Wolf, A., 2016. Bone Pose Estimation in the Presence of Soft Tissue Artifact Using Triangular Cosserat Point Elements. Ann. Biomed. Eng. 44, 1181–1190. doi:10.1007/s10439-015-1384-6

Solav, D., Rubin, M.B., Wolf, A., 2014. Soft Tissue Artifact compensation using Triangular Cosserat Point Elements (TCPEs). Int. J. Eng. Sci. 85, 1–9. doi:10.1016/j.ijengsci.2014.07.001

Spoor, C.W., Veldpaus, F.E., 1980. Rigid body motion calculated from spatial co-ordinates of markers. J.

Biomech. 13, 391–393. doi:10.1016/0021-9290(80)90020-2

Stagni, R., Fantozzi, S., 2009. Can cluster deformation be an indicator of soft tissue artefact? Gait Posture 30, S55. doi:10.1016/j.gaitpost.2009.07.050

Veldpaus, F.E., Woltring, H.J., Dortmans, L.J.M.G., 1988. A least-squares algorithm for the equiform transformation from spatial marker co-ordinates. J. Biomech. 21, 45–54. doi:10.1016/0021-9290(88)90190-X